What frequencies of standing surface waves can the subsolar magnetopause support?

M. O. Archer,[1]

and F. Plaschke,[2]

arXiv:1409.0383v4 [physics.space-ph] 23 Apr 2015

M. O. Archer, Space & Atmospheric Physics Group, The Blackett Laboratory, Imperial College London, Prince Consort Road, London, SW7 2AZ, UK. (m.archer10@imperial.ac.uk)

F. Plaschke, Space Research Institute, Austrian Academy of Sciences, 8042 Graz, Austria. (Ferdinand.Plaschke@oeaw.ac.at)

[1]Blackett Laboratory, Imperial College London, London, SW7 2AZ, UK.

[2]Space Research Institute, Austrian Academy of Sciences, 8042 Graz, Austria.

Abstract. It is has been proposed that the subsolar magnetopause may support its own eigenmode, consisting of propagating surface waves which reflect at the northern/southern ionospheres forming a standing wave. While the eigenfrequencies of these so-called Kruskal-Schwartzschild (KS) modes have been estimated under typical conditions, the potential distribution of frequencies over the full range of solar wind conditions is not know. Using models of the magnetosphere and magnetosheath applied to an entire solar cycle's worth of solar wind data, we perform time-of-flight calculations yielding a database of KS mode frequencies. Under non-storm times or northward interplanetary magnetic field (IMF), the most likely fundamental frequency is calculated to be $0.64^{+0.03}_{-0.12}$ mHz, consistent with previous estimates and indirect observational evidence for such standing surface waves of the subsolar magnetopause. However, the distributions exhibit significant spread (of order ± 0.3 mHz) demonstrating that KS mode frequencies, especially higher harmonics, should vary considerably depending on the solar wind conditions. The implications of such large spread on observational statistics are discussed. The subsolar magnetopause eigenfrequencies are found to be most dependent on the solar wind speed, southward component of the IMF and the *Dst* index, with the latter two being due to the erosion of the magnetosphere by reconnection and the former an effect of the expression for the surface wave phase speed. Finally, the possible occurrence of KS modes is shown to be controlled by the dipole tilt angle.

1. Introduction

Ultra-low frequency (ULF) waves in the Pc5 (2-7 mHz) range play a significant role in the mass, energy, and momentum transport within the Earth's magnetosphere e.g. through drift and bounce resonances with electrons in the outer radiation belt [*Claudepierre et al.*, 2013; *Mann et al.*, 2013]. Thus it is desirable to be able to predict the locations of magnetospheric ULF waves and, perhaps more importantly, their frequencies under the full range of solar wind conditions. The magnetosphere can support a number of resonantly excited ULF eigenmodes including: Field Line Resonances (FLRs), standing Alfvén waves on local field lines fixed at their ionospheric ends [e.g. *Southwood*, 1974]; and cavity or waveguide modes, radially standing fast mode waves trapped between magnetospheric boundaries or turning points [e.g. *Kivelson and Southwood*, 1985].

It has been proposed that the subsolar magnetopause may also support its own eigenmode which have been referred to as Kruskal-Schwartzschild (KS) modes, standing magnetopause surface waves or magnetopause surface eigenmodes [*Plaschke et al.*, 2009a; *Archer et al.*, 2013b]. A theory of these eigenmodes was developed by *Plaschke and Glassmeier* [2011], following on from work by *Kruskal and Schwartzschild* [1954] and *Chen and Hasegawa* [1974], using ideal magnetohydrodynamic (MHD) theory for incompressible plasmas in a box model magnetosphere. They consist of a pair of stable propagating surface waves (propagating parallel and antiparallel to the geomagnetic field) which reflect at the northern and southern ionospheres [*Plaschke et al.*, 2009a]. The superposition of these two surface waves results in a standing surface wave of the magnetopause, as illustrated in Figure 1, thereby quantising the possible resonance frequencies and forming an eigenmode

of the magnetopause. Note that these are unrelated to surface waves and vortices due to the Kelvin-Helmholtz instability, which typically occur far down the magnetopause flanks where large velocity shears are present [e.g. the review of *Johnson et al.*, 2014].

Standing magnetopause surface waves are thought to only be possible in the vicinity of the subsolar magnetopause, since the fast magnetosheath flow acts to convect surface waves tailward [e.g. *Pu and Kivelson*, 1983]. In order to establish an eigenmode of the magnetopause, the pair of oppositely propagating surface waves must be allowed to interfere with one another to form a standing wave. Away from the subsolar magnetopause, however, it is unlikely that the reflected surface waves would be able to propagate azimuthally against the opposing magnetosheath flow, thereby making standing surface waves not possible [*Plaschke and Glassmeier*, 2011]. Similarly, these reasons suggest that KS modes require small azimuthal wavenumbers.

While the subsolar magnetopause eigenmode shares a number of characteristics with FLRs, there are key differences. FLRs consist of toroidal or poloidal mode Alfvén waves which are localised to a field line, hence the eigenfrequencies of FLRs vary with L-shell/latitude [e.g. *Lee and Lysak*, 1989]. On the other hand, KS modes consist of magnetopause surface waves, which are theoretically described in MHD as two evanescent magnetosonic waves, one on the magnetosheath and the other on the magnetospheric side, tied together with boundary conditions [e.g. *Pu and Kivelson*, 1983]. Their magnetospheric signatures thus exponentially decay in amplitude with distance from the boundary. The eigenfrequencies of KS modes are characterised by the time it takes a disturbance at the magnetopause to propagate as a pair of surface waves to the northern/southern ionospheres, reflect back and then interfere with one another. This is in turn a function of the

physical properties of the magnetosheath and magnetospheric plasma along the path of the surface waves [*Chen and Hasegawa*, 1974]. *Plaschke et al.* [2009a] used typical magnetospheric and magnetosheath conditions at the nose, yielding an estimated fundamental eigenfrequency of ∼0.6 mHz. Subsequently, *Archer et al.* [2013b] used a similar method applied to 130 events showing that the eigenfrequencies (and moreso the surface wave phase speed) should correlate with the solar wind speed. However, such estimates of KS mode frequencies to date have not taken into account the full variability of the magnetospheric system. Furthermore, the calculations have used highly simplified box models of the magnetosheath-magnetosphere-ionosphere system whereby the plasma quantities have been assumed spatially constant and the effects of the magnetosheath flow ignored.

The first indirect observational evidence towards this ULF wave eigenmode was reported by *Plaschke et al.* [2009a] from a statistical set of observed subsolar magnetopause oscillation frequencies showing greater occurrence at some discrete frequencies, namely {1.3, 1.9, 2.7, 3.1, 4.1}±0.1 mHz. From the regularity of the observed frequencies it was inferred that these could possibly be explained as harmonics (integer multiples) of a fundamental eigenfrequency ∼0.65 mHz hence may be consistent with the expected KS mode frequencies. Boundary oscillations at these frequencies were found to occur more often under quasi-radial interplanetary magnetic field (IMF) [*Plaschke et al.*, 2009b]. Magnetosheath jets/dynamic pressure pulses are known to predominantly originate from the quasi-parallel bow shock i.e. quasi-radial IMF [*Archer et al.*, 2013a; *Plaschke et al.*, 2013] and it has been suggested that such localised pressure enhancements might be a natural driver for standing magnetopause surface waves [*Plaschke and Glassmeier*, 2011].*Archer et al.* [2013b] thus investigated the statistical reponse of the subsolar magnetosphere to

previously identified magnetosheath jets/dynamic pressure pulses [*Archer and Horbury*, 2013]. They found that the broadband jets indeed excited similar discrete frequencies, chiefly in the compressional component of the magnetic field, at geostationary orbit which they intepreted as further indirect evidence of KS modes.

It should be noted that comparable, possibly quasi-steady, discrete frequencies have been reported in a number of studies [*Fenrich et al.*, 1995; *Chisham and Orr*, 1997; *Francia and Villante*, 1997; *Villante et al.*, 2001; *Kokubun*, 2013]. These have been attributed to different modes, depending on the circumstances of the observations (location, solar wind conditions etc.), such as cavity/waveguide modes in the flank magnetosphere [*Samson et al.*, 1991, 1992]; waves across the dayside directly driven by solar wind dynamic pressure oscillations [*Kepko et al.*, 2002; *Kepko and Spence*, 2003; *Viall et al.*, 2008]; or pulsed reconnection at the subsolar magnetopause due to oscillations of the IMF direction [*Prikryl et al.*, 1998, 1999]. Some statistical studies have shown little evidence for predominant discrete quasi-steady frequencies though [*Baker et al.*, 2003; *Rae et al.*, 2012]. It is therefore of interest to theoretically estimate the distribution of possible discrete frequencies due to the different known modes under the full range of solar wind and magnetospheric conditions. In this paper we restrict ourselves to just one of these modes, the eigenmode of the subsolar magnetopause, performing time-of-flight calculations applied to more representative models of the magnetosphere and magnetosheath than previous studies. Thus we estimate, for the first time, the distribution of KS mode eigenfrequencies over an entire solar cycle, revealing their most likely set of eigenfrequencies and quantifying how variable these should be in general. We also investigate what parameters primarily

control the possible occurrence and frequency of these modes, determining the physical explanation for these dependences.

2. Method

2.1. Data & Models

We use 5 min resolution solar wind data (in GSM coordinates where appropriate) from the OMNI database between 2001-2013, spanning an entire solar cycle. OMNI combines observations from numerous spacecraft to produce an estimate of the solar wind conditions at the bow shock nose. There were 1,262,690 datapoints during this period. To estimate the frequencies of standing surface waves that the subsolar magnetopause may support, we combine a number of physics-based and semi-empirical models of magnetosheath and magnetospheric properties which are summarised in Table 1. These models are applied to the subsolar magnetopause field line (also known as the last closed field line) from the T96 magnetospheric magnetic field model [*Tsyganenko*, 1995; *Tsyganenko and Stern*, 1996]. While the KF94 [*Kobel and Flückiger*, 1994] magnetosheath magnetic field model contains a different explicitly defined boundary to T96, we connect them together through the solar zenith angle. Furthermore, in the polar cusps the magnetic field and density are interpolated between the magnetosheath and magnetospheric values as a function of geocentric distance from the extrema (triangles in Figure 2) to 60% of this distance [c.f. *Lavraud et al.*, 2004]. We also reduce the magnetosheath flow speed to zero within 10% of the distance from the extrema.

2.2. KS Mode Frequency Calculation

In this paper we estimate the fundamental frequencies of standing surface waves at the subsolar magnetopause, assuming that their wavevectors $\mathbf{k} = k_\mu \boldsymbol{\mu} + k_\nu \boldsymbol{\nu} + k_\phi \boldsymbol{\phi}$ (where $\boldsymbol{\mu}$ is along the T96 geomagnetic field, $\boldsymbol{\nu}$ is normal to the field line pointing outwards and $\boldsymbol{\phi}$ is the usual azimuthal direction) have vanishing azimuthal component i.e. $k_\phi = 0$, such that the surface waves do not propagate downtail (see section 5.1 for more discussion). Using incompressible MHD, the local dispersion relation for a magnetopause surface wave is given by [c.f. *Plaschke and Glassmeier*, 2011]

$$(\rho_{msh} + \rho_{sph}) \left(\frac{\omega}{k_\mu}\right)^2 - 2\rho_{msh} u_{msh} \left(\frac{\omega}{k_\mu}\right) + \rho_{msh} u_{msh}^2 - \rho_{msh} v_{A,msh}^2 \cos^2\theta_B - \rho_{sph} v_{A,sph}^2 = 0 \tag{1}$$

where the subscripts msh and sph correspond to the magnetosheath and magnetospheric sides of the boundary respectively, $\rho = m_p n$ is the mass density assuming a purely proton composition, u is the velocity, v_A is the Alfvén speed, θ_B is the magnetic shear angle between the magnetosheath and magnetospheric fields, and ω is the angular frequency of the wave. While we account for the Doppler effect of the magnetosheath flow, we assume that velocities inside the magnetosphere are negligible. Since Equation 1 is quadratic, there are two analytical solutions to the phase speed $\omega/k_\mu = c_\pm$, corresponding to surface waves propagating parallel (+) or antiparallel (−) to the geomagnetic field as illustrated in Figure 1. Using the T96 model, we determine positions along the subsolar magnetopause field line and compute the two phase speeds at each point using the models given in Table 1. A worked example is given in Figure 2.

Since standing waves must consist of both parallel and anti-parallel propagating surface waves which reflect at the northern and southern ionospheres (see Figure 1), if the propagation direction of either of these surface waves is reversed in Earth's rest frame at some point along the field line (due to the magnetosheath flow) then a KS mode cannot be supported [*Plaschke and Glassmeier*, 2011]. On the other hand, when this does not occur we arrive at the fundamental standing surface wave frequency f_{KS} using the time-of-flight technique

$$f_{KS} \equiv \left[\sum_{\pm} \int \frac{ds}{c_{\pm}} \right]^{-1} \tag{2}$$

where ds is a differential line element along the field line. We assess the validity of these calculations given the models and assumptions used in section 5.1.

3. Occurrence

We investigate the conditions which control the possible occurrence of standing surface waves at the subsolar magnetopause by plotting histograms of the fraction of the time that they were unsupported (due to a reversal of the phase speed by the magnetosheath flow making the surface wave unable to reach its target ionosphere) as a function of the model inputs. Overall, KS modes were allowed 61% of the time in our model, corresponding to 765,553 computed frequencies. We find that the main controlling parameter of KS mode occurrence is the dipole tilt angle, as shown in Figure 3 (left). For small tilt angles standing surface waves are largely allowed, whereas they are generally unsupported at large tilt angles. Furthermore, it is the parallel propagating wave which is reversed (blue) for positive dipole tilts and the antiparallel wave (red) for negative tilts.

Here we try to understand this dependence on dipole tilt theoretically. From Equation 1 it follows that KS modes are unsupported due to the reversal of either the parallel or antiparallel surface wave by the magnetosheath flow if at any point along the field line

$$0 \geq -\rho_{msh} u_{msh}^2 + \rho_{sph} v_{A,sph}^2 + \rho_{msh} v_{A,msh}^2 \cos^2\theta_B \tag{3a}$$

$$\Rightarrow 0 \geq -P_{dyn,msh} + 2P_{B,sph} + 2P_{B,msh}\cos^2\theta_B \tag{3b}$$

$$\Rightarrow 0 \geq -\frac{P_{dyn,msh}}{P_{dyn,sw}} + \frac{2P_{B,sph}}{P_{dyn,sw}} + \frac{2P_{B,msh}\cos^2\theta_B}{P_{dyn,sw}} \equiv \delta \tag{3c}$$

where the subscript sw refers to the solar wind, $P_{dyn} = \rho u^2$ is the dynamic pressure, P_B is the magnetic pressure and we introduce the parameter δ which becomes negative when one of the waves is reversed. The *Spreiter et al.* [1966] models of the magnetosheath density and flow are proportional to their respective solar wind conditions, thus the first term in Equation 3c is a function of solar zenith angle only. For simplicity, here we consider the second term using pressure balance [e.g. *Spreiter et al.*, 1966] applied to the KF94 magnetopause model, which again makes this term solely dependent on the solar zenith angle. While the third term does vary with the upstream conditions, it is typically small. We therefore plot the parameter δ in Figure 3 (bottom right) as a function of solar zenith angle for a representative range of the third term. This shows that δ decreases with increasing solar zenith angle, becoming zero at ∼60-70°. Therefore, if one of the polar cusps are located at a similarly large solar zenith angle then KS modes will be unsupported due to a reversal of one of the surface waves.

Figure 3 (top right) shows the solar zenith angles of the intersection of the northern (red) and southern (blue) cusps with the KF94 magnetopause model as a function of the dipole tilt angle, assuming a constant invariant latitude of the polar cusps of ±78°

[*Russell*, 2000]. For zero dipole tilt, both cusps are located at zenith angles of $\sim 50^\circ$ where δ is positive and thus standing surface waves at the subsolar magnetopause are supported. For $+30^\circ$ dipole tilt, the southern cusp is located at a large solar zenith angle $\sim 75^\circ$ where δ has become negative. Here the magnetosheath flow is in opposition to the parallel propagating wave (as seen in the right inset of Figure 3) hence this wave is reversed and a KS mode is not possible. Similarly, for -30° dipole tilt it is the northern cusp at a large zenith angle where the magnetosheath flow opposes the anti-parallel wave (illustrated in the left inset) thereby reversing it. This simple theoretical treatment is therefore in agreement with the determined dependence of KS mode occurrence on dipole tilt angle in the full model.

4. Frequencies

4.1. Results

4.1.1. Distributions

Figure 4 (top left) shows distributions of the calculated fundamental standing surface wave frequencies of the subsolar magnetopause. We have separated all the computed frequencies by geomagnetic activity using a Dst threshold of -10 nT, close to the median value, to distinguish between storm (grey; 393,958 datapoints) and non-storm (black; 371,595 datapoints) times. In addition we separate all the frequencies under northward (red; 287,266 datapoints) or southward (blue; 478,287 datapoints) interplanetary magnetic field (IMF). The distributions show the correctly normalised probability density functions (PDFs) i.e. the probability that f_{KS} was between f and $f + df$ is given by $PDF\,(f)\,df$ such that the area under each PDF is unity.

We find that under non-storm times or northward IMF the most likely frequency is 0.64 mHz. Given the vast number of samples in our distributions and the insensitivity of the result with different bin sizes, we have high statistical confidence that this is the mode, i.e. the most likely value, of our model calculations. The accuracy of our calculations are later discussed in section 5.1. This is consistent with the ∼0.65 mHz fundamental suggested by *Plaschke et al.* [2009a] (indicated by the vertical dashed line). In contrast, during storm times or under southward IMF the most likely frequency is greater (more so for the former), hence inconsistent with previous estimates. Note that the computed fundamental FLR frequencies for the same field line are much larger, typically by a factor of ∼3-6.

The distributions are highly skewed, as evidenced by the medians being larger than the modes in all cases. Indeed, this must be the case since negative frequencies are not possible. In fact, the distributions shown in Figure 4 can be fairly well modelled as log-normal (not shown). It is clear that all the distributions show significant spread as evidenced by their interquartile ranges (IQRs). This spread, which is of the order of ±0.3 mHz (∼50% the most likely value) in the cases of non-storm times or northward IMF and much larger otherwise, is significant. Therefore, while we quote a most likely frequency of 0.64 mHz, frequencies outside this range should often occur. For instance in our model distributions 0.64 mHz is only 35% more likely than either 0.5 mHz or 0.8 mHz during non-storm times, but ∼30 times more likely than 0.1 mHz or 1.5 mHz.

We also wish to understand the time variability of the subsolar magnetopause eigenfrequencies. We therefore construct waiting time distributions for absolute changes in f_{KS} greater than some threshold percentage. Fitting these to a negative exponential distribu-

tion, we find that 20% changes (used here since it is greater than the presumed accuracy of the calculations as discussed in section 5.1) in the frequency occur after a characteristic timescale of 48 min. Increasing the frequency change threshold by successive 10% increments results in further factor ∼1.75 increases in the characteristic waiting times. We thus conclude that KS mode frequencies should be relatively stable over the time of wave propagation.

4.1.2. Dependences

To ascertain whether the KS mode frequency is predominantly an average phase speed or field line length effect, we plot bivariate histograms of f_{KS} against the reciprocal of the field line length $S \equiv \int ds$ and the average phase speed $\langle c_{\pm} \rangle \equiv 2Sf_{KS}$ in Figure 4(top right). The average phase speed was found to be typically ∼1.3 times larger than the phase speed at the nose, used in previous frequency calculations [*Plaschke et al.*, 2009a; *Plaschke and Glassmeier*, 2011; *Archer et al.*, 2013b]. Since the correlation coefficient is susceptible to skewness and outliers, we use the correlation median estimator R [*Pasman and Shevlyakov*, 1987; *Falk*, 1998] to assess the dependences. While both the field line length and average phase speed do affect f_{KS} as indicated by the medians (black lines), the correlation shows the average phase speed dominates.

The average phase speed can be thought of as a mean weighted by the time-of-flight of the surface waves, thus we introduce a generalised weighted average given by

$$\langle a \rangle \equiv \left[\sum_{\pm} \int \frac{a}{c_{\pm}} ds \right] / \left[\sum_{\pm} \int \frac{ds}{c_{\pm}} \right] \tag{4}$$

and determine which of the magnetospheric or magnetosheath Alfvén speeds (where only the component of the latter along the geomagnetic field line is used) is most important in

prescribing f_{KS}. The bivariate histograms of these are also shown in Figure 4 (top right) revealing high correlation in both quantities, though the magnetosheath Alfvén speed correlates better hence KS mode frequencies are slightly more dependent on magnetosheath properties than those in the magnetosphere.

Figure 4 (bottom) shows bivariate histograms of f_{KS} against the input parameters (spanning 0.5-99.5%) to our calculations. We find that the fundamental KS mode frequency depends most strongly on the solar wind speed, disturbance storm time index (Dst) when negative and southward component of the IMF. All other variables correlate poorly and the slope of the medians (black) are small for the majority of the data, indicating little dependence.

We perform a multiple linear regression on the fundamental standing surface wave frequency, where we normalise the input parameters x_i by subtracting their median values and dividing by the interquartile range i.e.

$$f_{KS} = a_0 + \sum_i a_i \left[\frac{x_i - \mathrm{Med}\,(x_i)}{\mathrm{IQR}\,(x_i)} \right] \tag{5}$$

where a_0 is a constant. The coefficients a_i of the regression give a measure of the partial derivative of the frequency (keeping all other variables fixed) to each variable whereas the previous correlations relate to the total derivatives. The resulting regression coefficients (as well as the normalisations) are shown in Table 2. While the residuals of this linear model are comparable to the spread of the distribution of f_{KS} and thus should not be used to estimate the frequency, it does nonetheless reveal the relative dependences of the inputs on the frequency. Again we see that southward IMF, the solar wind speed and the

Dst index affect f_{KS} the most, with all other variables having order of magnitude smaller coefficients.

4.2. Interpretation

Here we interpet the physics governing the dependences discovered in the previous section.

4.2.1. u_{sw} dependence

Archer et al. [2013b] also discovered a dependence of expected standing surface wave frequencies of the subsolar magnetopause on the solar wind speed for 130 subsolar magnetosheath jet events, with this high correlation being an effect of the phase speed at the nose (the assumed constant phase speed over the entire field line). The phase speed of a surface wave at the magnetopause nose is given by

$$c_0 = \sqrt{\frac{B_{msh,0}^2 \cos^2\theta_B + B_{sph,0}^2}{\mu_0\left(\rho_{msh,0}+\rho_{sph,0}\right)}} \qquad \begin{matrix} B_{sph,0} \gg B_{msh,0} \\ \rho_{msh,0} \gg \rho_{sph,0} \end{matrix} \tag{6a}$$

$$\simeq \sqrt{\frac{B_{sph,0}^2}{\mu_0 \rho_{msh,0}}} \qquad \begin{matrix} B_{sph,0}^2/2\mu_0 = \rho_{sw} u_{sw}^2 \\ \rho_{msh,0} \sim 4.23\rho_{sw} \end{matrix} \tag{6b}$$

$$\simeq 0.69 u_{sw} \tag{6c}$$

demonstrating the approximate linear relation with solar wind speed. A least-squares linear fit of the calculated nose phase speed from our model results in a coefficient of 0.739, consistent with that from our simple derivation, and we find a correlation $R = 0.88$. Since c_0 also highly correlates with the average phase speed ($R = 0.84$), this explains the strength of the determined relationship of the frequency with solar wind speed ($0.88 \times 0.84 \times 0.91 = 0.67$ is close to the $R = 0.61$ correlation of f_{KS} with u_{sw}).

4.2.2. $B_{z,sw} < 0$ and Dst dependences

Here we consider both the southward component of the IMF and Dst dependences on the fundamental KS mode frequency. These two variables are not entirely independent, with large negative values of Dst indicating storm times typically occurring during times of southward IMF [*Burton et al.*, 1975]. Nonetheless, there are times (about 16% of all observations) when Dst indicates storm times whereas the IMF is northward. Similarly, 27% of all times we find that the IMF is southward yet Dst indicates non-storm times. Since Dst and $B_{z,sw}$ are both inputs to our model and are determined separately, with the GSM z component of the IMF measured in the solar wind and Dst determined from ground magnetometer measurements, we have thus far treated them independently in our statistical analyses.

We interpret the dependence of the fundamental standing surface wave frequency on the southward component of the IMF as being due to the T96 model's parameterisation of the erosion of the dayside magnetosphere by reconnection. *Dungey* [1961] described how reconnection leads to shrinkage of the dayside magnetopause and a transport of magnetic flux from the dayside to the nightside, resulting in equatorward motion of the cusps [e.g. *Burch*, 1973; *Newell et al.*, 1989]. Therefore, under southward IMF the shape of the subsolar magnetopause field line is changed whereby the standoff distance is shorter and the field line is less extended in the GSM z direction. This can be seen in the examples shown in Figure 5 for both northward and southward IMF keeping all other inputs constant. While the field line is shorter under southward IMF, which will have the effect of increasing the fundamental frequency, we have already established that the average phase speed is more important in terms of the frequency. The typical reduction of the magnetospheric and magnetosheath magnetic fields near the cusps won't be as large

for southward IMF since the field lines do not extend as far in the z direction. This effect can clearly be seen in Figure 5. The overall effect is that the average magnetic fields on both sides of the boundary over the field line are increased compared to northward IMF, thereby increasing the Alfvén speeds (the average densities are barely affected) resulting in higher frequencies.

The disturbance storm time index measures the intensity of the ring current, whereby negative values mean that Earth's magnetic field is weakened. The primary causes of geomagnetic storms are strong dawn-dusk electric fields associated with the passage of southward IMF, with reconnection providing the energy transfer between the IMF and the magnetosphere [e.g. *Gonzalez et al.*, 1994]. Therefore during storm times, identified by strong negative Dst, the dayside magnetosphere will again be eroded. Example calculations varying Dst but keeping all other inputs constant (not shown) are indeed very similar to those varying only $B_{z,sw}$. We therefore interpret the effect of negative Dst on the fundamental KS mode frequency to also be due to the T96 model's parameterisation of this erosion.

5. Discussion

5.1. Validity of calculations

Here we discuss the validity and accuracy of our KS mode fundamental eigenfrequency calculations, in particular how known effects not captured in this study may affect our results. These are summarised in Table 3 where the median percentage differences are given along with standard deviations.

Firstly we assess the dependence of the computed frequencies on the specific magnetosheath and magnetospheric model quantities used in this paper through sensitivity tests

i.e. changing the models used and their parameters [c.f. *Berube et al.*, 2006; *McCollough et al.*, 2008]. The computed frequencies are largely insensitive to the precise models used as previously noted by *Archer et al.* [2013b] e.g. altering the magnetospheric density by a factor of 2 affects f_{KS} by less than 3%, in contrast to FLRs whose frequencies are highly dependent on the magnetospheric mass density [e.g. *Waters et al.*, 1996]. Overall we estimate the accuracy of the computed frequencies due to the choice of models used to be $\sim \pm 10\%$.

The time-of-flight technique used in this paper essentially relies on the WKB approximation to the solution of the full wave equation. However, since the wavelengths in consideration for the fundamental eigenfrequency are comparable to or larger than, for example, the scale size of density and magnetic field variations along a field line (e.g. Figure 2) this is not strictly justified [*Singer et al.*, 1981; *Schulz*, 1996; *Rankin et al.*, 2006; *Kabin et al.*, 2007]. This effect has been shown to be small, but not negligible, for FLRs applied to similar models to those here through numerically solving the full wave equation in the model geometry [e.g. *Wild et al.*, 2005]. Thus the use of time-of-flight analysis in this study may affect the exact numerical solutions. It can be shown by inserting the assumed WKB solution into a general wave equation that, to the next order, a correction factor to the time-of-flight integral in Equation 2 applies, given by [e.g. *Kroemer*, 1994]

$$\sqrt{1 + \frac{1}{2}\frac{k''_\mu}{k_\mu} - \frac{3}{4}\left(\frac{k'_\mu}{k_\mu}\right)^2} \tag{7}$$

where primes indicate the spatial derivative along the field line. Calculating this correction factor reveals it alters our frequency estimates by $+15 \pm 4\%$ i.e. a reasonably systematic effect on our results.

On a similar note, the time-of-flight calculations were applied to a local dispersion relation whereas the subsolar magnetopause field line is clearly curved. *Singer et al.* [1981] derived a wave equation, applied to standing Alfvén waves, in a generalised magnetic field geometry through the introduction of a geometry-dependent scale factor h_α, the relative normal distance between field lines given some initial displacement vector (see also *Rankin et al.* [2006] and *Kabin et al.* [2007]). It can be easily shown from the resulting wave equation that while these spatially varying h_α factors affect the local amplitudes and damping rates of waves, it has no effect on the phase (and thus no effect on the wave frequency in a time-of-flight calculation). Therefore our results are not changed by this consideration.

The surface wave dispersion relation used in this study (Equation 1) assumes there is no azimuthal component to the wavevector. This is justifiable because a surface wave with a significant azimuthal component to its group velocity $\partial\omega/\partial\mathbf{k}$ will be convected tailward down the flanks by the fast magnetosheath flow (see Figure 1). As discussed in the introduction, standing surface waves are likely not possible away from the subsolar magnetopause, though KS modes could perhaps be supported with some azimuthal propagation. We therefore assess the change in the total surface wave phase speed at the magnetopause nose by introducing a small k_ϕ, finding this has little effect ($-0.5 \pm 0.4\%$ for $k_\phi = 0.1k_\mu$) on our results.

Our calculations also assume plasma incompressibility, however *Plaschke and Glassmeier* [2011] showed that this isn't strictly valid at the magnetopause using typical conditions. We assess the validity of the incompressibility assumption here using the parameter

$$\frac{K^2}{k_\mu^2} \equiv \frac{\omega^2}{v_A^2 + c_s^2\left[\omega^2 - (\mathbf{k}\cdot\mathbf{v}_A)^2\right]/\omega^2} \tag{8}$$

whereby incompressibility is valid if $\left|K^2/k_\mu^2\right| \ll 1$ [*Plaschke and Glassmeier*, 2011]. Using the results of our analysis, this is estimated at each point along the field line as

$$\frac{K_{msh}^2}{k_\mu^2} = \frac{c_\pm^2 \left(1 \mp \frac{u_{msh}}{c_\pm}\right)^2}{v_{A,msh}^2 + c_{s,msh}^2 \left[\left(1 \mp \frac{u_{msh}}{c_\pm}\right)^2 - \frac{v_{A,msh}^2}{c_\pm^2}\cos^2\theta_B\right] / \left(1 \mp \frac{u_{msh}}{c_\pm}\right)^2} \tag{9a}$$

$$\frac{K_{sph}^2}{k_\mu^2} = \frac{c_\pm^2}{v_{A,sph}^2 + c_{s,sph}^2 \left[1 - \frac{v_{A,sph}^2}{c_\pm^2}\right]} \tag{9b}$$

The sound speed c_s is computed in the magnetosphere by assuming a plasma β of 0.15 [e.g. *Phan et al.*, 1994] and in the magnetosheath by pressure balance i.e. the magnetosheath thermal pressure is given by $(1 + \beta_{sph}) \times$ the magnetic pressure of T96 minus the magnetic pressure of the KF94 draping model. Figure 6 shows a bivariate histogram of the average values of $\left|K^2/k_\mu^2\right|$ over the field lines in both the magnetosheath (horizontal axis) and magnetosphere (vertical axis), where the logarithmic colour scale indicates the number of datapoints in each bin. The medians, first (25%) and third (75%) quartiles are also indicated for both the magnetosheath and magnetosphere. It is clear that the incompressibility assumption $\left|K^2/k_\mu^2\right| \ll 1$ is generally valid in the magnetosphere but not in the magnetosheath. The full compressible plasma dispersion relation is a 10th order polynomial for which no general analytical solution exists, hence it would have to be solved numerically at each point on the field line. This would result in multiple solutions corresponding to different modes (e.g. S and F modes [*Pu and Kivelson*, 1983]) which would have to be carefully identified and matched together at each point, making the calculation of KS mode frequencies much more difficult. To assess the effect magnetosheath plasma compressibility has on our results, we construct a new dispersion relation applicable at the magnetopause nose where the compressible plasma relation is included for

the magnetosheath only. This yields a quartic equation in the square of the surface wave phase speed which is solved numerically and any positive real solutions (corresponding to stable surface waves) are compared with the phase speed from Equation 1. We find that taking account of magnetosheath compressibility also has a reasonably systematic effect on our results, adjusting them by $-20 \pm 4\%$.

When the magnetic shear θ_B between the draped IMF and the geomagnetic field is small, plasma depletion can occur resulting in increased magnetic fields and reduced plasma densities on the magnetosheath side of the boundary [*Zwan and Wolf*, 1976]. The width of this plasma depletion layer (PDL) depends on the Alfvénic Mach number of the bow shock M_A, with large PDL's being possible under low M_A. Our models do not include a PDL, which would serve to increase the magnetosheath Alfvén speed, thereby increasing the KS mode frequency from those estimated here. Using the results of *Paschmann et al.* [1993], we find that plasma depletion should modify our calculations by $+60 \pm 20\%$. However, this process should only be prevalent $\sim$1% of the time overall ($\theta_B < 30^\circ$ and $M_A < 8$), hence does not significantly alter our statistical results.

Finally, if reconnection is occurring at any point along the subsolar magnetopause field line, then the magnetosphere will be open and standing surface waves will not be possible. We have not accounted for the occurrence of reconnection in our distributions, though of course this will not affect our results under northward IMF. Using its $\Delta\beta$-θ_B dependence [*Swisdak et al.*, 2010; *Phan et al.*, 2013] we estimate reconnection was allowed at most 64% of the time under southward IMF. Note that this is a necessary but not a sufficient condition in establishing whether reconnection may be occurring at any time in our calculations. Nonetheless, removing these times we find that the spread of our distribu-

tions for storm times and under southward IMF are reduced by 0.1-0.2 mHz and that the most likely frequency under southward IMF becomes 0.7 mHz. These are relatively small changes to our results, which have mostly concentrated on the unaffected northward IMF and non-storm times anyway.

Combining all of these effects on our calculations, we estimate that the overall accuracy of the results presented here is $^{+4}_{-19}$%. Future modelling work into standing surface waves of the subsolar magnetopause should attempt to incorporate some or all these effects fully to give a more accurate description of the eigenmode. Many of these considerations, however, will necessitate significantly more computationally intensive calculations, hence may not be suitable for such a large statistical database as that presented here. A number of case studies should thus be modelled and the eigenfrequencies found may then be compared with those presented here.

5.2. Implications

The results of our calculations provide a database of expected fundamental frequencies of KS modes at the subsolar magnetopause, given the magnetospheric and solar wind conditions at each time. The possible eigenfrequencies of the subsolar magnetopause at any given time thus correspond to integer multiples of this fundamental frequency f_{KS} i.e. the harmonics of the standing surface waves are qf_{KS} where $q \in \mathbb{N}$. Using the most likely frequency under both northward IMF and non-storm times, this corresponds to {0.6, 1.3, 1.9, 2.6, 3.2...} mHz, consistent with the reported discrete frequencies interpreted as indirect evidence of KS modes [*Plaschke et al.*, 2009a; *Archer et al.*, 2013b].

However, our distributions of f_{KS} (Figure 4 top left) exhibit significant spread (of order 50%), which should result in a large range of frequencies for the higher harmonics. Indeed,

the error bars in Figure 7 indicate the interquartile ranges of the first 7 harmonics of KS modes from our non-storm time calculations, revealing much overlap in frequency between the different harmonics. We therefore wish to understand what effect the significant spread in the fundamental frequency would have on observational statistics. We use two different simple methods to approximate the distributions of oscillation frequencies due to standing surface waves of the subsolar magnetopause that could potentially be observed:

1. Assume that the first 7 harmonics are present at all times
2. Randomly choose just one of the first 7 harmonics at each time

Both of these methods produce frequency distributions (shown in Figure 7) whereby the most likely fundamental frequency of 0.64 mHz shows a prominant peak, whereas no further significant peaks are found i.e. the overtones of the most likely fundamental eigenfrequency are not apparent in these occurence distributions. Therefore, while our results suggest a most likely set of KS mode eigenfrequencies may exist, they also predict that occurrence distributions of Pc5 frequencies due to KS modes would actually result in a continuum. This is in contrast to the results of *Plaschke et al.* [2009b] showing prominant observed oscillation frequencies of the subsolar magnetopause which were then attributed to KS modes. There are, however, a couple of possible explanations why discrete frequencies due to subsolar magnetopause eigenmodes may occur in such statistical studies. If statistics are poor and therefore do not cover the full range of solar wind conditions or there is some unconscious selection bias towards certain solar wind conditions, then the sample distribution of frequencies may not be representative of the full distribution. It is thus possible that distinct peaks may emerge under these circumstances. An alternative explanation comes down to the presence or not of a suitable driver. Our distributions

make no predictions on whether standing surface waves may actually be present at the subsolar magnetopause at any given time. Such a statement would require consideration of some particular driver for this eigenmode such as solar wind pressure pulses or localised magnetosheath jets [*Archer et al.*, 2013b]. If such a driver existed at some time, then the KS modes could be excited at one of the harmonics of our calculated fundamental frequency f_{KS} or a combination thereof. However, such drivers may preferentially occur under certain solar wind conditions. Indeed, *Plaschke et al.* [2009b] found that subsolar magnetopause oscillations tended to occur under low cone-angle IMF, conditions for which magnetosheath jets predominantly occur [*Archer and Horbury*, 2013; *Plaschke et al.*, 2013].

Since magnetopause surface waves are evanescent in the magnetosphere, their signatures should decay exponentially with distance from the boundary. Assuming incompressibility, typically valid on the magnetospheric side of the boundary as shown in section 5.1, we have $k^2 \equiv k_\nu^2 + k_\phi^2 + k_\mu^2 = 0$ [*Plaschke and Glassmeier*, 2011] and thus in our calculations the magnitude of the (imaginary) radial component of the wavevector$|k_\nu| = |k_\mu|$. The evanescent length scale at the magnetopause nose is therefore given by $|k_\nu|^{-1} = c_0/(2\pi q f_{KS})$, where q is again the harmonic number of the KS mode. We calculate this length scale for the most likely KS mode harmonics during non-storm times (with frequencies given earlier) yielding {8.5, 4.2, 2.8, 2.14, 1.7...} R_E. Thus while the higher harmonics are somewhat confined to the vicinity of the subsolar magnetopause, the first few harmonics could potentially be detected at, for example, geostationary orbit. Previous work has shown that discrete Pc5 oscillation frequencies in the subsolar magnetosphere at geostationary orbit can be explained as directly driven waves 54% of the time that periodic

density structures exist in the solar wind [*Viall et al.*, 2009]. However, discrete compressional Pc5 oscillations have also been observed due to broadband magnetosheath jets in the absence of such monochromatic solar wind dynamic pressure fluctuations and these have been interpreted as KS modes [*Archer et al.*, 2013b]. While the results presented here suggest this interpretation is indeed plausible, the current indirect observational evidence for KS modes should be carefully reassessed in the context of this study to ascertain whether those observed frequencies can indeed be explained as due to this eigenmode of the subsolar magnetopause. While KS modes have been proposed as a potential source of discrete field line resonances in general [*Plaschke et al.*, 2009a], whether such coupling can occur at some location inside the subsolar magnetosphere will be highly dependent on the FLR frequency profile within the KS mode's spatially confined extent. It is unclear at present how often such coupling may occur, which is beyond the scope of this study but could form the basis of future work. However, we limit our discussions, analysis and implications of standing subsolar surface waves of the magnetopause to the subsolar region only and make no claim that these oscillations can directly excite discrete FLRs in the magnetospheric flanks, such as those reported by *Samson et al.* [1991, 1992].

6. Conclusions

In this paper we have presented the first estimates of the distribution of standing surface wave frequencies at the subsolar magnetopause using the time-of-flight technique [e.g. *Wild et al.*, 2005] applied to combined models of the magnetosphere and magnetosheath. We find that the most likely frequency during non-storm times or under northward IMF is $0.64^{+0.03}_{-0.12}$ mHz, consistent with the fundamental frequency of $\sim$0.65 mHz proposed by *Plaschke et al.* [2009a] from a simple estimate using typical conditions and the approx-

imate regularity of observed oscillation periods of the subsolar boundary. However, the distributions exhibit a large amount of spread (of order ± 0.3 mHz or 50%), sufficient that the overtones of the most likely frequency are not apparent when constructing distributions of the KS mode harmonics over the full range of solar wind conditions.

We find that the KS mode frequencies principally depend on the solar wind speed, in agreement with *Archer et al.* [2013b], as well as the disturbance storm time (Dst) index and the southward component of the IMF. We have ascertained the physical reasons for these dependences, with the latter two being due to the erosion of the dayside magnetosphere by reconnection and the solar wind speed dependence a result of the phase speed of surface waves at the magnetopause nose (in turn proportional to the average phase speed). Finally, we present that the possible occurrence of KS modes (reconnection notwithstanding) is primarily controlled by the dipole tilt angle, since the reversal of either the parallel or antiparallel propagating surface waves by the magnetosheath flow is predominantly a geometrical effect.

Future work will compare the magnetospheric ULF wave activity in spacecraft and ground magnetometer data with our database of expected KS mode frequencies. It is clear though that care must be taken for example in identifying harmonics in the observations and accounting for all possible ULF wave drivers and modes for each event. By doing this it may be possible to not only validate our model calculations, but provide further evidence for the possible existence of eigenmodes of the subsolar magnetopause.

Acknowledgments. M. O. Archer is thankful for funding through STFC grant ST/I505713/1. The OMNI data was obtained from the NASA/GSFC OMNIWeb inter-

face at http://omniweb.gsfc.nasa.gov. We thank the editor for their helpful suggestions during the review process.

References

Archer, M. O., and T. S. Horbury, Magnetosheath dynamic pressure enhancements: Occurrence and typical properties, *Ann. Geophys.*, *31*, 319–331, doi:10.5194/angeo-31-319-2013, 2013.

Archer, M. O., T. S. Horbury, J. P. Eastwood, J. M. Weygand, and T. K. Yeoman, Magnetospheric response to magnetosheath pressure pulses: A low pass filter effect, *J. Geophys. Res.*, *118*, 5454–5466, doi:10.1002/jgra.50519, 2013a.

Archer, M. O., M. D. Hartinger, and T. S. Horbury, Magnetospheric "magic" frequencies as magnetopause surface eigenmodes, *Geophys. Res. Lett.*, *40*, 5003–5008, doi:10.1002/grl.50979, 2013b.

Baker, G. J., E. F. Donovan, and B. J. Jackel, A comprehensive survey of auroral latitude Pc5 pulsation characteristics, *J. Geophys. Res.*, *108*, SMP 11–1, doi:10.1029/2002JA009801, 2003.

Berube, D., M. B. Moldwin, and M. Ahn, Computing magnetospheric mass density from field line resonances in a realistic magnetic field geometry, *J. Geophys. Res*, *111*, A08,206, doi:10.1029/2005JA011450, 2006.

Burch, J. L., Rate of erosion of dayside magnetic flux based on a quantitative study of the dependence of polar cusp latitude on the interplanetary magnetic field, *Radio Sci.*, *8*, 955–961, doi:10.1029/RS008i011p00955, 1973.

Burton, R. K., R. L. McPherron, and C. T. Russell, An empirical relationship between interplanetary conditions and dst, *J. Geophys. Res.*, *80*, 4204–4214, doi: 10.1029/JA080i031p04204, 1975.

Chen, L., and A. Hasegawa, A theory of long-period magnetic pulsations: 2. impulse excitation of surface eigenmode, *J. Geophys. Res.*, *79*, 1033–1037, doi: 10.1029/JA079i007p01033, 1974.

Chisham, G., and D. Orr, A statistical study of the local time asymmetry of Pc5 ULF wave characteristics observed at midlatitudes by SAMNET, *J. Geophys. Res.*, *102*, 24,339–24,350, doi:10.1029/97JA01801, 1997.

Claudepierre, S. G., et al., Van Allen Probes observation of localized drift resonance between poloidal mode ultra-low frequency waves and 60 keV electrons, *Geophys. Res. Lett.*, *40*, 4491–4497, doi:10.1002/grl.50901, 2013.

De Keyser, J., M. W. Dunlop, C. J. Owen, B. U. . Sonnerup, S. E. Haaland, A. Vaivads, G. Paschmann, R. Lundin, and L. Rezeau, Magnetopause and boundary layer, *Space Science Reviews*, *118*, 231–320, doi:10.1007/s11214-005-3834-1, 2005.

Denton, R. E., J. Goldstein, J. D. Menietti, and S. L. Young, Magnetospheric electron density model inferred from Polar plasma wave data, *J. Geophys. Res.*, *107*, SMP 25–1 – SMP 25–8, doi:10.1029/2001JA009136, 2002.

Dungey, J. W., Interplanetary magnetic field and the auroral zones, *Phys. Rev. Lett.*, *6*, 47–48, doi:10.1103/PhysRevLett.6.47, 1961.

Falk, M., A note on the co-median for elliptical distributions, *J. Multivar. Analysis*, *67*, 306–317, doi:10.1006/jmva.1998.1775, 1998.

Fenrich, F. M., J. C. Samson, G. Sofko, and R. A. Greenwald, ULF high- and low-m field line resonances observed with the Super Dual Auroral Radar Network, *J. Geophys. Res.*, *100*, 21,535–21,547, doi:10.1029/95JA02024, 1995.

Francia, P., and U. Villante, Some evidence of ground power enhancements at frequencies of global magnetospheric modes at low latitude, *Ann. Geophys.*, *15*, 17–23, doi:10.1007/s00585-997-0017-2, 1997.

Gonzalez, W. D., J. A. Joselyn, Y. Kamide, H. W. Kroehl, G. Rostoker, B. T. Tsurutani, and V. M. Vasyliunas, What is a geomagnetic storm?, *J. Geophys. Res.*, *99*, 5771–5792, doi:10.1029/93JA02867, 1994.

Johnson, J. R., S. Wing, and P. A. Delamere, Kelvin helmholtz instability in planetary magnetospheres, *Space Sci. Rev.*, *184*, 1–31, doi:10.1007/s11214-014-0085-z, 2014.

Kabin, K., R. Rankin, C. L. Waters, R. Marchand, E. F. Donovan, and J. C. Samson, Different eigenproblem models for field line resonances in cold plasma: Effect on magnetospheric density estimates, *Planet. Space Sci.*, *55*, 820–828, doi:10.1016/j.pss.2006.03.014, 2007.

Kepko, L., and H. E. Spence, Observations of discrete, global magnetospheric oscillations directly driven by solar wind density variations, *J. Geophys. Res.*, *108*, SMP21–1 – SMP21–12, doi:10.1029/2002JA009676, 2003.

Kepko, L., H. E. Spence, and H. J. Singer, ULF waves in the solar wind as direct drivers of magnetospheric pulsations, *Geophys. Res. Lett.*, *29*, 39–1 – 39–4, doi:10.1029/2001GL014405, 2002.

Kivelson, M. G., and D. J. Southwood, Resonant ULF waves: a new interpretation, *Geophys. Res. Lett.*, *12*, 49–52, doi:10.1029/GL012i001p00049, 1985.

Kobel, E., and E. O. Flückiger, A model of the steady state magnetic field in the magnetosheath, *J. Geophys. Res.*, *99*, 23,617–23,622, doi:10.1029/94JA01778, 1994.

Kokubun, S., ULF waves in the outer magnetosphere: Geotail observation 1 transverse waves, *Earth Planets Space*, *65*, 411–433, doi:10.5047/eps.2012.12.013, 2013.

Kroemer, H., *Quantum Mechanics for Engineering, Materials Science and Applied Physics*, Prentice Hall, 1994.

Kruskal, M., and M. Schwartzschild, Some instabilities of a completely ionized plasma, *Proc. R. Soc. London, Ser. A.*, *223*, 348–360, doi:10.1098/rspa.1954.0120, 1954.

Landau, L., and E. Lifshitz, *Fluid Mechanics*, Pergamon Press, 1959.

Lavraud, B., A. Fedorov, E. Budnik, A. Grigoriev, P. J. Cargill, M. W. Dunlop, H. RÃšme, I. Dandouras, and A. Balogh, Cluster survey of the high-altitude cusp properties: a three-year statistical study, *Ann. Geophys.*, *22*, 3009–3019, doi:10.5194/angeo-22-3009-2004, 2004.

Lee, D.-H., Dynamics of MHD wave propagation in the low-latitude magnetosphere, *J. Geophys. Res.*, *101*, 15,371–15,386, doi:10.1029/96JA00608, 1996.

Lee, D.-H., and R. L. Lysak, Magnetospheric ULF wave coupling in the dipole model: The impulsive excitation, *J. Geophys. Res.*, *94*, 17,097–17,103, doi:10.1029/JA094iA12p17097, 1989.

Mann, I. R., et al., Discovery of the action of a geophysical synchrotron in the Earth's Van Allen radiation belts, *Nature Commun.*, *4*, 2795, doi:10.1038/ncomms3795, 2013.

McCollough, J. P., J. L. Gannon, D. N. Baker, and M. Gehmeyr, A statistical comparison of commonly used external magnetic field models, *Space Weather*, *6*, S10,001, doi:10.1029/2008SW000391, 2008.

Newell, P. T., C.-I. Meng, and D. G. Sibeck, Some low-altitude cusp dependencies on the interplanetary magnetic field, *J. Geophys. Res.*, *94*, 8921–8927, doi: 10.1029/JA094iA07p08921, 1989.

Paschmann, G., W. Baumjohann, N. Sckopke, T. D. Phan, and H. Lühr, Structure of the dayside magnetopause for low magnetic shear, *J. Geophys. Res.*, *98*, 13,409–13,422, doi:10.1029/93JA00646, 1993.

Pasman, V., and G. L. Shevlyakov, Robust estimation of a correlation coefficient, *Avtomat. Telemekh.*, *3*, 70–80, 1987.

Phan, T. D., G. Paschmann, W. Baumjohann, N. Sckopke, and H. Lühr, The magnetosheath region adjacent to the dayside magnetopause: AMPTE/IRM observations, *J. Geophys. Res.*, *99*, 121–141, doi:10.1029/93JA02444, 1994.

Phan, T. D., G. Paschmann, J. T. Gosling, M. Oieroset, M. Fujimoto, J. F. Drake, and V. Angelopoulos, The dependence of magnetic reconnection on plasma β and magnetic shear: Evidence from magnetopause observations, *Geophys. Res. Lett.*, *40*, 11–16, doi: 10.1029/2012GL054528, 2013.

Plaschke, F., and K. H. Glassmeier, Properties of standing kruskal-schwarzschild-modes at the magnetopause, *Ann. Geophys.*, *29*, 1793–1807, doi:10.5194/angeo-29-1793-2011, 2011.

Plaschke, F., K.-H. Glassmeier, H. U. Auster, O. D. Constantinescu, W. Magnes, V. Angelopoulos, D. G. Sibeck, and J. P. McFadden, Standing alfvÃ©n waves at the magnetopause, *Geophys. Res. Lett.*, *36*, L02,104, doi:10.1029/2008GL036411, 2009a.

Plaschke, F., K.-H. Glassmeier, D. G. Sibeck, H. U. Auster, O. D. Constantinescu, V. Angelopoulos, and W. Magnes, Magnetopause surface oscillation frequencies at different

solar wind conditions, *Ann. Geophys.*, *27*, 4521–4532, doi:10.5194/angeo-27-4521-2009, 2009b.

Plaschke, F., H. Hietala, and V. Angelopoulos, Anti-sunward high-speed jets in the subsolar magnetosheath, *Ann. Geophys.*, *31*, 1877–1889, doi:10.5194/angeo-31-1877-2013, 2013.

Prikryl, P., R. A. Greenwald, G. J. Sofko, J. P. Villain, C. W. S. Ziesolleck, and E. Friis-Christensen, Solar-wind-driven pulsed magnetic reconnection at the dayside magnetopause, pc5 compressional oscillations, and field line resonance, *J. Geophys. Res*, *103*, 17,307–17,322, doi:10.1029/97JA03595, 1998.

Prikryl, P., J. W. MacDougall, I. F. Grant, D. P. Steele, G. J. Sofko, and R. A. Greenwald, Observations of polar patches generated by solar wind alfvén wave coupling to the dayside magnetosphere, *Ann. Geophys.*, *17*, 463–489, doi:10.1007/s00585-999-0463-0, 1999.

Pu, Z.-Y., and M. G. Kivelson, Kelvin-Helmholtz Instability at the magnetopause: Solution for compressible plasmas, *J. Geophys. Res.*, *88*, 841–852, doi:10.1029/JA088iA02p00841, 1983.

Rae, I. J., I. R. Mann, K. R. Murphy, L. G. Ozeke, D. K. Milling, A. A. Chan, S. R. Elkington, and F. Honary, Ground-based magnetometer determination of in situ Pc4-5 ULF electric field wave spaectra as a function of solar wind speed, *J. Geophys. Res.*, *117*, A04,221, doi:10.1029/2011JA017335, 2012.

Rankin, R., K. Kabin, and R. Marchand, Alfvénic field line resonances in arbitrary magnetic field topology, *Adv. Space Res.*, *38*, 1720–1729, doi:10.1016/j.asr.2005.09.034, 2006.

Russell, C. T., The polar cusp, *Adv. Space Res.*, *25*, 1413–1424, doi:10.1016/S0273-1177(99)00653-5, 2000.

Samson, J. C., R. A. Greenwald, J. M. Ruohoniemi, T. J. Hughes, and D. D. Wallis, Magnetometer and radar observations of magnetohydrodynamic cavity modes in the Earth's magnetosphere, *Can. J. Phys.*, *69*, 929–937, doi:10.1139/p91-147, 1991.

Samson, J. C., B. G. Harrold, J. M. Ruohoniemi, R. A. Greenwald, and A. D. M. Walker, Field line resonances associated with MHD waveguides in the magnetosphere, *Geophys. Res. Lett.*, *19*, 441–444, doi:10.1029/92GL00116, 1992.

Schulz, M., Eigenfrequencies of geomagnetic field lines and implications for plasma-density modeling, *J. Geophys. Res.*, *101*, 17,385–17,397, doi:10.1029/95JA03727, 1996.

Shue, J.-H., et al., Magnetopause location under extreme solar wind conditions, *J. Geophys. Res.*, *103*, 17,691–17,700, doi:10.1029/98JA01103, 1998.

Singer, H. J., D. J. Southwood, R. J. Walker, and M. G. Kivelson, Alfvén wave resonances in a realistic magnetospheric magnetic field geometry, *J. Geophys. Res.*, *86*, 4589–4596, doi:10.1029/JA086iA06p04589, 1981.

Southwood, D. J., Some features of field line resonances in the magnetosphere, *Planet. Space Sci.*, *22*, 483–491, doi:10.1016/0032-0633(74)90078-6, 1974.

Spreiter, J. R., A. L. Summers, and A. Y. Alksne, Hydromagnetic flow around the magnetosphere, *Planet. Space Sci.*, *14*, 223–250, doi:10.1016/0032-0633(66)90124-3, 1966.

Swisdak, M., M. Opher, J. F. Drake, and F. Alouani Bibi, The vector direction of the interstellar magnetic field outside the heliosphere, *Ap. J.*, *710*, 1769–1775, doi:10.1088/0004-637X/710/2/1769, 2010.

Tsyganenko, N. A., Modeling the earth's magnetospheric magnetic field confined within a realistic magnetopause, *J. Geophys. Res.*, *100*, 5599–5612, doi:10.1029/94JA03193, 1995.

Tsyganenko, N. A., and D. P. Stern, Modeling the global magnetic field of the large-scale Birkeland current systems, *J. Geophys. Res.*, *101*, 27,187–27,198, doi:10.1029/96JA02735, 1996.

Viall, N. M., L. Kepko, and H. E. Spence, Inherent length-scales of periodic solar wind number density structures, *J. Geophys. Res.*, *113*, A07,101, doi:10.1029/2007JA012881, 2008.

Viall, N. M., L. Kepko, and H. E. Spence, Relative occurrence rates and connection of discrete frequency oscillations in the solar wind density and dayside magnetosphere, *J. Geophys. Res.*, *114*, A01,201, doi:10.1029/2008JA013334, 2009.

Villante, U., P. Francia, and S. Lepidi, Pc5 geomagnetic field fluctuations at discrete frequencies at a low latitude station, *Ann. Geophys.*, *19*, 321–325, doi:10.5194/angeo-19-321-2001, 2001.

Waters, C. L., J. C. Samson, and E. F. Donovan, Variation of plasmatrough density derived from magnetospheric field line resonances, *J. Geophys. Res.*, *101*, 24,737–24,745, doi:10.1029/96JA01083, 1996.

Wild, J. A., T. K. Yeoman, and C. L. Waters, Revised time of flight calculations for high latitude geomagnetic pulsations using a realistic magnetospheric magnetic field model, *J. Geophys. Res.*, *110*, A11,206, doi:10.1029/2004JA010964, 2005.

Zwan, B. J., and R. A. Wolf, Depletion of solar wind plasma near a planetary boundary, *J. Geophys. Res.*, *81*, 1636–1648, doi:10.1029/JA081i010p01636, 1976.

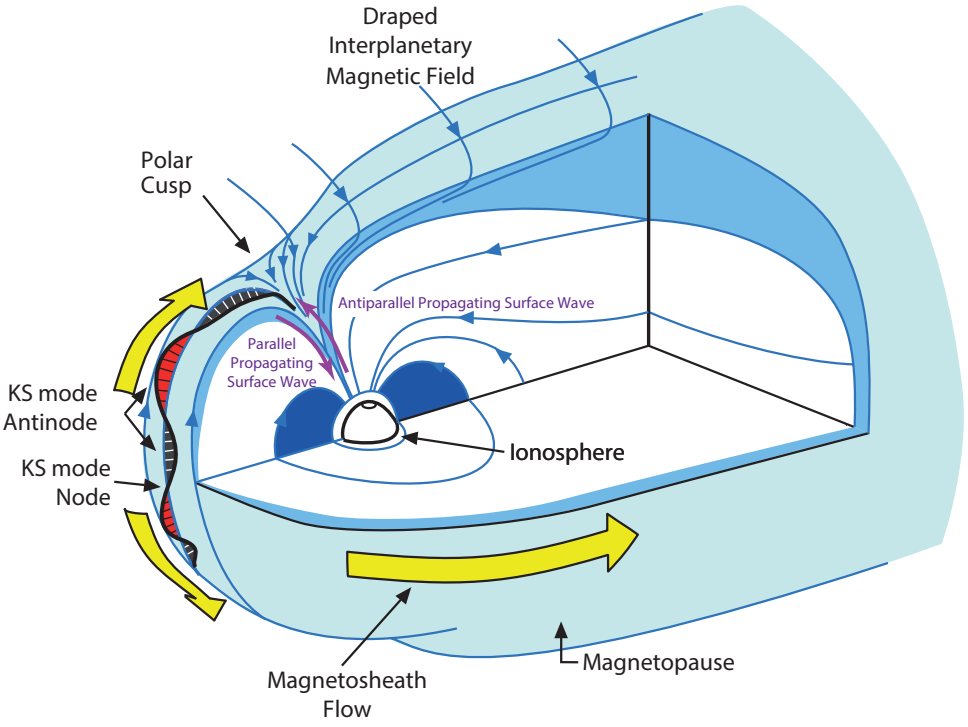

Figure 1: Illustration of standing surface waves at the subsolar magnetopause, known as Kruskal-Schwartzschild (KS) modes. Adapted from *De Keyser et al.* [2005].

Quantity	Model	Model Inputs
$\mathbf{B}_{sph}$	T96	$P_{dyn,sw}$, $B_{y,sw}$, $B_{z,sw}$, Dst, Dipole Tilt
$\mathbf{B}_{msh}$	KF94	$\mathbf{B}_{sw}$, $r_{mp,0}$, $r_{bs,0}$
n_{sph}	Power Law $n = n_0 \left(r_{mp,0}/r\right)^m$	$m = 2$ [*Denton et al.*, 2002] n_0 =1 cm^{-3} [e.g. *Lee*, 1996]
n_{msh}	*Spreiter et al.* [1966]	n_{sw}
u_{msh}	*Spreiter et al.* [1966]	u_{sw}
$r_{mp,0}$	*Shue et al.* [1998]	$P_{dyn,sw}$, $B_{z,sw}$
$r_{bs,0}$	*Landau and Lifshitz* [1959]	$r_{mp,0}$, M_{ms}

Table 1: Summary of the models used in this study.

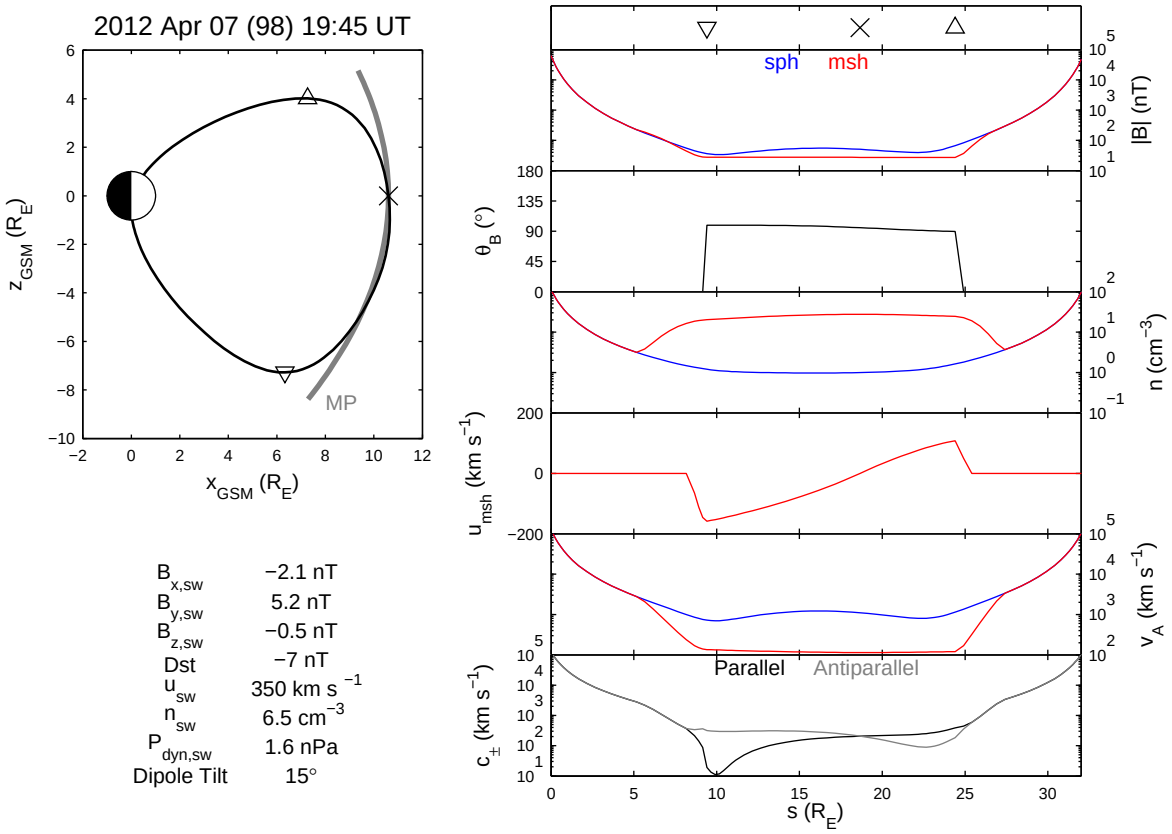

Figure 2: Example KS mode frequency calculation. Left**:** Subsolar magnetopause field line (black) from the T96 magnetospheric magnetic field model in the GSM x-z plane. The subsolar point (cross) and extrema (triangles) of the field line are also indicated. The paraboloidal magnetopause used for the KF94 magnetosheath magnetic field model is also shown (grey). Right: magnetic field strengths; magnetic shear angle; number densities; magnetosheath flow speeds; Alfvén speeds; and surface wave phase speeds for the parallel (black) and antiparallel (grey) propagating surface waves. Model quantities are shown as a function of length along the field line from the southern footpoint to the northern. Values on the magnetospheric and magnetosheath sides of the boundary are shown in blue and red respectively. The calculated fundamental frequency here was $f_{KS} = 0.49$ mHz.

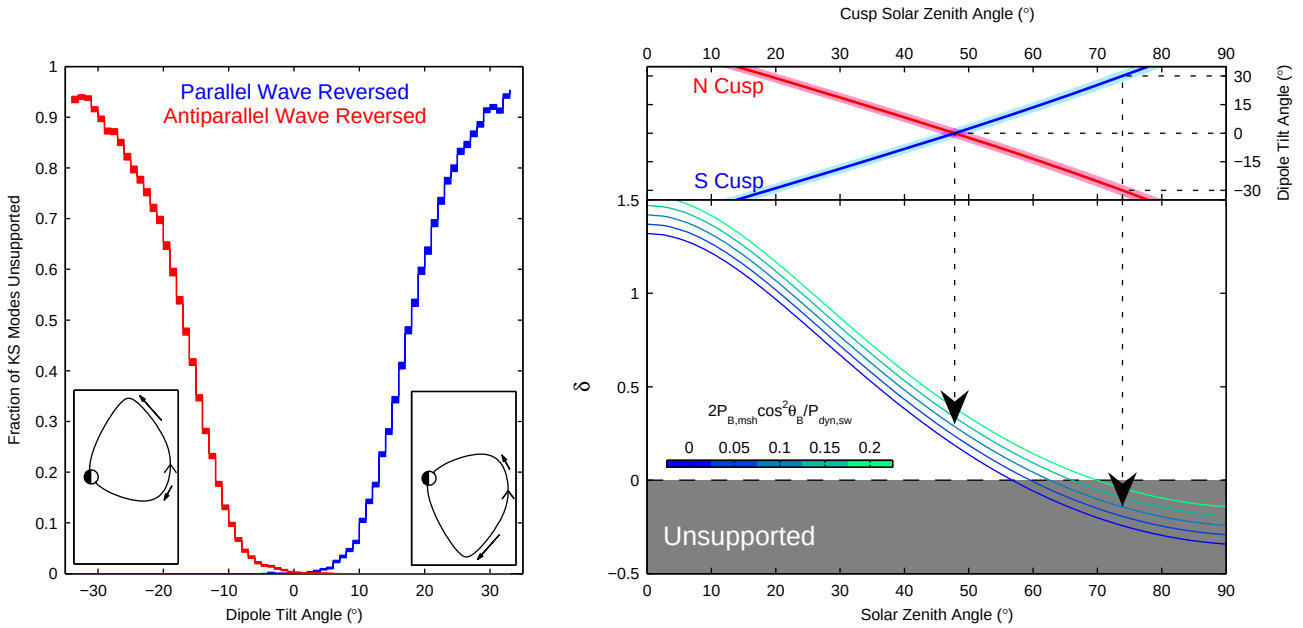

Figure 3: Left: Fraction of KS modes unsupported (due to reversal by the magnetosheath flow) as a function of the dipole tilt angle due to the parallel (blue) or antiparallel (red) propagating surface waves being reversed by the magnetosheath flow. The height of the bars indicates the 95% confidence intervals. Inset are examples of the T96 subsolar magnetopause field line in the x-z GSM plane for negative (left inset) and positive (right inset) tilt, with the magnetosheath flow and geomagnetic field direction also indicated. Right: The solar zenith angle locations of the northern (red) and southern (blue) cusps as a function of dipole tilt angle are shown in the top panel. The lines show results for a magnetopause standoff distance of $10\,R_E$, with the shaded regions indicating $\pm 1\,R_E$. The bottom panel shows the variation of the parameter δ defined in Equation 3c, whereby $\delta \leq 0$ means that KS modes are unsupported, for a representative range of values of $2P_{B,msh}\cos^2\theta_B/P_{dyn,sw}$ given by the colour scale.

Variable	Med	IQR	a_i (mHz)
a_0	-	-	0.687
$B_{x,sw}$	0.16 nT	5.03 nT	-0.006 $B_{x,sw} < 0$ -0.006 $B_{x,sw} \geq 0$
$B_{y,sw}$	-0.16 nT	5.00 nT	$+0.022$ $B_{y,sw} < 0$ -0.027 $B_{y,sw} \geq 0$
$B_{z,sw}$	0.03 nT	3.47 nT	-0.375 $B_{z,sw} < 0$ $+0.031$ $B_{z,sw} \geq 0$
Dst	-8 nT	19 nT	-0.199 $Dst < 0$ -0.112 $Dst \geq 0$
u_{sw}	413 km s^{-1}	142 km s^{-1}	0.299
n_{sw}	4.45 cm^{-3}	4.08 cm^{-3}	0.013
$P_{dyn,sw}$	1.60 nPa	1.26 nPa	0.018

Table 2: Results of the multiple linear regression model defined in Equation 5. The standard deviation of the residuals was 0.25 mHz.

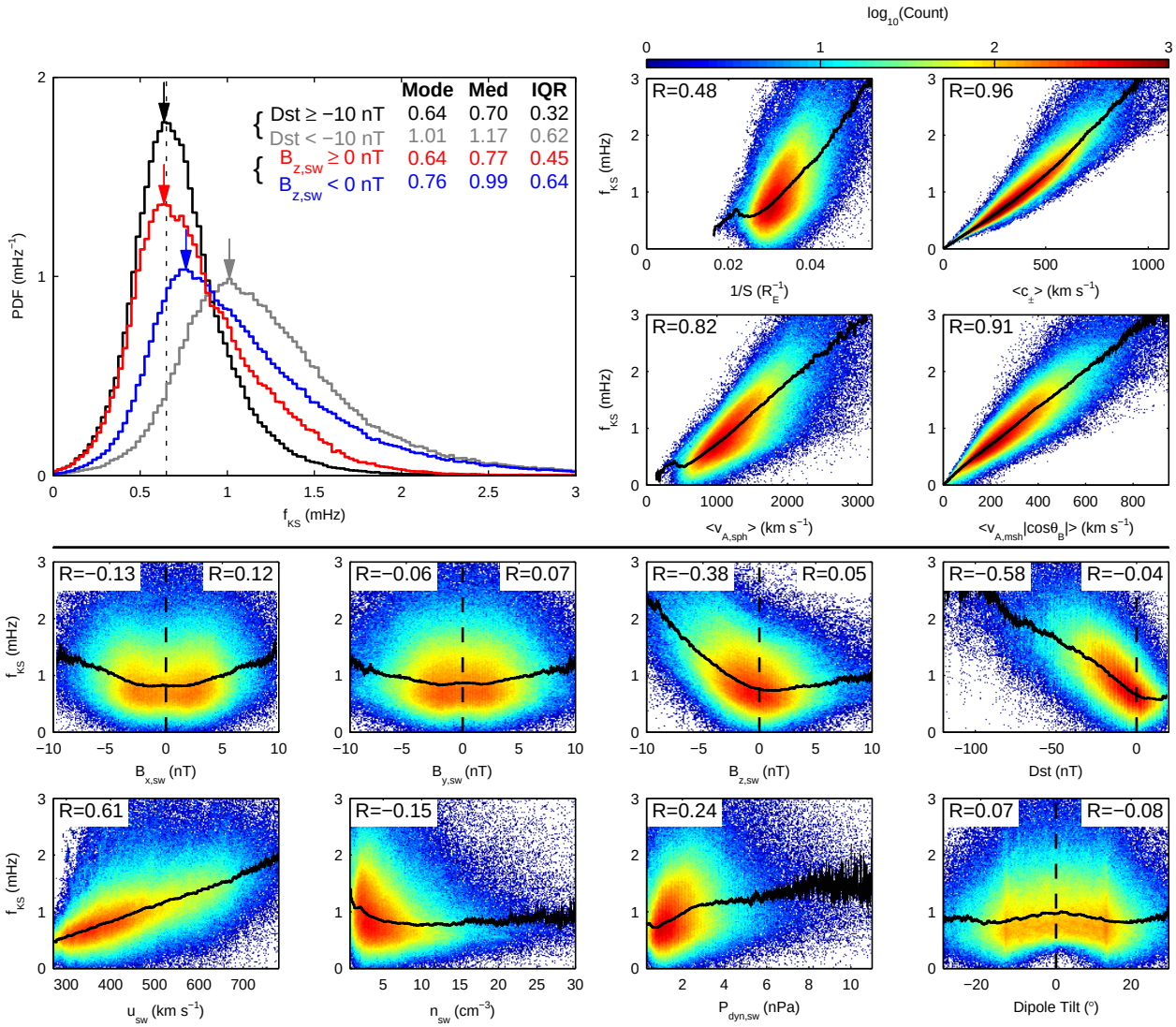

Figure 4: Top Left: Distribution of calculated fundamental KS mode frequencies during storm (grey) and non-storm (black) times and under northward (red) and southward (blue) IMF respectively. The mode (indicated by the arrows), median and interquartile range are also given for each. The vertical dotted line is at 0.65 mHz. Top Right: Bivariate histograms showing the dependence of the fundamental KS mode frequency on the (reciprocal of the) field line length, average phase speed, average magnetospheric Alfvén speed and the average magnetosheath Alfvén speed projected along the geomagnetic field direction. The logarithmic colour scale shows the number of datapoints in each bin and the black line indicates the median frequency for each horizontal bin. Bottom: Bivariate histograms in the same format showing the dependence of the fundamental KS mode frequency on the input parameters - GSM x, y and z components of the IMF, the *Dst* index, solar wind speed, density, dynamic pressure and the dipole tilt angle.

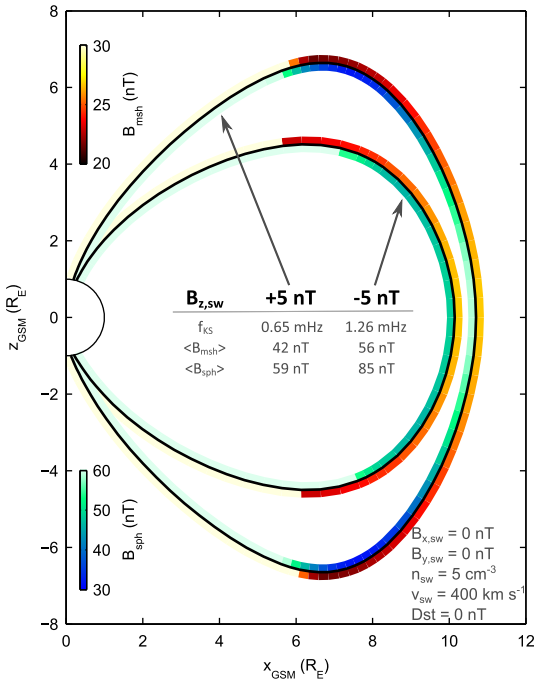

Figure 5: Examples of T96 subsolar magnetopause field lines under northward and southward IMF (black) with all other inputs kept constant. The colours either side of the field line represent the magnetic field strength on the magnetospheric and magnetosheath sides of the boundary, from the T96 and KF94 models respectively.

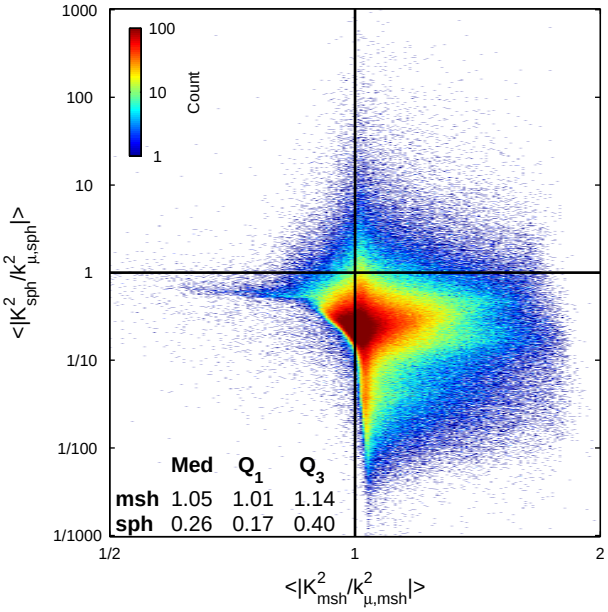

Figure 6: Bivariate histogram of the average values of $\left|K^2/k_\mu^2\right|$ over the field lines, used to assess the incompressibility assumption, in both the magnetosheath (horizontal axis) and magnetosphere (vertical axis). The logarithmic colour scale indicates the number of datapoints in each bin. The medians, first (25%) and third (75%) quartiles are also indicated for both the magnetosheath and magnetosphere.

Approximation	Region of inapplicability	Effect on f_{KS}
Model Quantities	-	$\pm 10\%$
WKB	-	$+15 \pm 4\%$
$k_\phi = 0$	-	$-0.5 \pm 0.4\%$
Incompressibility	Magnetosheath	$-20 \pm 4\%$
No PDL	Low θ_B & M_A ($\sim 1\%$ of time)	$+60 \pm 20\%$
No Reconnection	$< 64\%$ of time for $B_{z,sw} < 0$	Unsupported
Overall Accuracy of Model Calculations		$^{+4}_{-19}$ %

Table 3: Summary of the approximations in our model calculations and estimates of their effects (including the spread) on the fundamental frequency calculations.

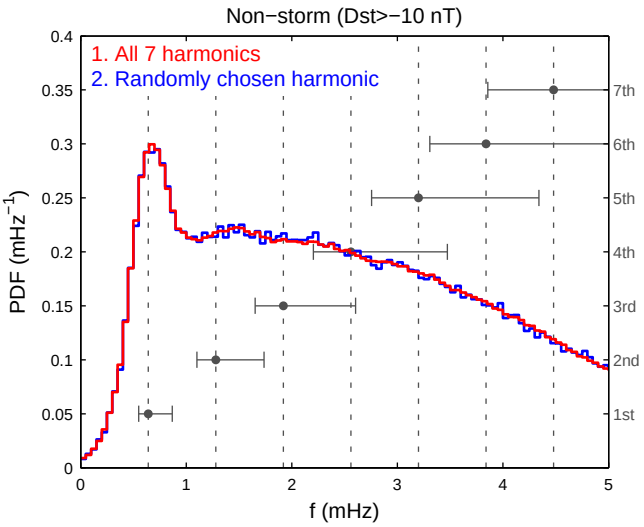

Figure 7: Estimates of oscillation frequency occurrence distributions due to KS mode harmonics during non-storm times, assuming either: 1. all 7 harmonics are present at all times (red) or 2. one randomly chosen harmonic is present at each time (blue). The harmonics (integer multiples) of the most likely fundamental frequency (c.f. Figure 4 top left) are shown as the vertical dotted lines, with the error bars indicating their interquartile ranges.